Plasmon spectrum of two-dimensional electron systems with Rashba spin-orbit interaction

X. F. Wang*
Department of Physics, Concordia University, 1455 de Maisonneuve Ouest, Montréal, Québec, Canada H3G 1M8
(Received 8 September 2004; revised manuscript received 19 April 2005; published 4 August 2005)

The dielectric function and plasmon modes of a two-dimensional electron gas (2DEG) are studied in single- and double-quantum-well structures with Rashba spin-orbit interaction (RSOI) in the framework of the random-phase approximation. The RSOI splits each parabolic energy subband of a 2DEG into two nonparabolic spin branches and affects the electronic many-body correlation and dielectric properties of the 2DEG. The influence of the RSOI on the 2DEG plasmon spectrum in single quantum wells appears mainly in three ways: (1) an overall frequency lowering due to the energy band deformation; (2) a weak frequency oscillation stemming from the spin-split energy band; and (3) an enhancement of the Landau damping as a result of the emerging of the interbranch single-particle-excitation spectrum. In double quantum wells, the above effects are enhanced for the optic plasmon mode but diminished for the acoustic one.

DOI: 10.1103/PhysRevB.72.085317 PACS number(s): 73.21.−b, 71.45.Gm, 85.75.−d, 72.25.−b

I. INTRODUCTION

The growing interest in spintronics is leading to an extensive exploration of electronic properties of a two-dimensional electron gas (2DEG) in semiconductor heterostructures with spin-orbit interaction (SOI) thanks to its promising application in manipulating spins.[1,2] As a relativistic effect of dynamic electrons moving in an electric field, the intrinsic SOI exists in bulk semiconductors with structural inversion asymmetry,[3] while controllable SOI can be introduced by asymmetrically confining a 2DEG in semiconductor heterostructures to create an average electric field across the electron system. In general, the former results in the cubic Dresselhaus term of the SOI and the latter introduces the Rashba term for isotropic 2DEG and the anisotropic linear Dresselhaus term.[4–6] In some narrow-gap semiconductors, such as InGaAs, the Rashba spin-orbit interaction (RSOI) dominates and can be well controlled in the laboratory.[7] In the past several years many authors addressed the RSOI effects on one-body ballistic transport but the study of the RSOI effects on many-body properties of 2DEG is relatively limited. As is well known, dielectric properties and plasmon spectrum can reveal fundamental many-body correlations in a 2DEG. In the presence of the RSOI they have been discussed in the literature.[8–12] However, some authors concluded that the charge plasmon spectrum is not affected by the RSOI (Ref. 10) and others declared the splitting of the plasmon spectrum in the presence of RSOI.[9,12]

From an experimental point of view, the double-quantum-well (DQW) structure is a good candidate for studying the electron correlation and collective modes of a 2DEG through transport measurements such as Coulomb drag. In a DQW system composed of two spatially separated quantum wells without tunneling, the two 2DEGs, which are coupled with each other via Coulomb interaction, may oscillate collectively out of phase or in phase. The former case corresponds to the lower frequency acoustic plasmon and the latter to the optic plasmon.[13–17] Both plasmon modes play an important role in the many-body properties and enhance significantly the Coulomb drag in bilayer systems.[18–21] In this paper we focus on the effects of the RSOI on the plasmon modes in single-quantum-well (SQW) and DQW systems.

II. DIELECTRIC FUNCTION

We consider two Coulomb-coupled 2DEGs without tunneling in a DQW structure of a narrow gap semiconductor, InGaAs/InAlAs, where the RSOI due to confinement along the z direction dominates. An effective mass $m^*=0.05m_0$, with m_0 the free electron mass, and the background dielectric constant $\epsilon_\infty=10.8$ are assumed. In each well the one-electron Hamiltonian of the 2DEG, in the x-y plane, is expressed as

$$\hat{H}=\frac{\hat{\mathbf{p}}^2}{2m^*}+V(z)+\frac{\alpha}{\hbar}(\hat{\sigma}\times\hat{\mathbf{p}})_z. \tag{1}$$

The parameter α measures the RSOI strength and is proportional to the average interface electric field, $V(z)$ is the electric confinement potential along the z direction, $\hat{\sigma}=(\sigma_x,\sigma_y,\sigma_z)$ denotes the spin Pauli matrices, and $\hat{\mathbf{p}}$ is the momentum operator. The eigenstates of the Schrödinger equation $\hat{H}\Psi(\mathbf{r})=E\Psi(\mathbf{r})$ are readily obtained as

$$\Psi_{\mathbf{k}}^{\sigma}(\mathbf{r})=\psi(z)\frac{e^{i\mathbf{k}\cdot\mathbf{r}}}{\sqrt{2}}\begin{pmatrix}1\\ e^{i\phi_{\mathbf{k}}^{\sigma}}\end{pmatrix} \tag{2}$$

with $\mathbf{k}\equiv(k_x,k_y)$, $\mathbf{r}\equiv(x,y)$, and $e^{i\phi_{\mathbf{k}}^{\sigma}}=\sigma(k_y-ik_x)/k$; $k=\sqrt{k_y^2+k_x^2}$ is the radial wave vector and $\sigma=\pm1$ denotes the electron spin in the + (upper) or − (lower) branch. $\psi(z)$ is the wave function along the z direction. $\phi_{\mathbf{k}}^{\sigma}$ is the angle between the x axis and the direction of the spin polarization, which is perpendicular to the electronic wave vector in the 2D plane as shown by the arrows along the Fermi circles in Fig. 1.

The eigenvalues corresponding to the eigenstates $(\mathbf{k},\sigma)$ are

$$E^{\sigma}(\mathbf{k})=\frac{\hbar^2}{2m^*}k^2+\sigma\alpha k. \tag{3}$$

This rotationally symmetric electron energy spectrum, E^{σ} vs $\mathbf{k}$, is illustrated in Fig. 1 for a strength $\alpha=5\alpha_0$ and an elec-

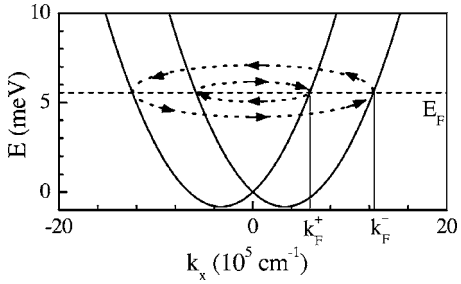

FIG. 1. Energy spectrum of a 2DEG with RSOI. The two dotted ellipses at the Fermi energy E_F illustrate the rotational symmetry in x-y plane of the two Fermi circles of the + and − spin branches. The arrows tangent to the Fermi circles indicate the spin directions.

tron density $n_e=1.5n_0$, with $\alpha_0=10^{-11}$ eV m and $n_0=10^{11}$ cm^{-2}. The Fermi wave vector of the spin branch σ is $k_F^\sigma=\sqrt{2\pi n_e-k_\alpha^2}-\sigma k_\alpha$ with $k_\alpha=\alpha m^*/\hbar^2$.

Equations (1)–(3) apply to each well when the interwell coupling is neglected and a well index, i or j, will be introduced in the following when the coupling is taken into account. With the help of Eq. (2), we obtain directly the bare Coulomb interaction between an electron $(\mathbf{k},\sigma)$ in well i and another one $(\mathbf{p},\sigma_1)$ in well j. As shown diagrammatically in Fig. 2(a), its Fourier transformation reads

$$v_{ij,\mathbf{k},\mathbf{p}}^{\sigma,\sigma',\sigma_1,\sigma_1'}(\mathbf{q})=g_i^{\sigma,\sigma'}(\mathbf{k},\mathbf{k}+\mathbf{q})v_{ij}(q)g_j^{\sigma_1,\sigma_1'}(\mathbf{p},\mathbf{p}-\mathbf{q}), \quad (4)$$

where

$$v_{ij}(q)=\int d\mathbf{r}e^{i\mathbf{q}\mathbf{r}}\int dz\int dz'|\psi_i(z)|^2|\psi_j(z')|^2e^2/(4\pi\epsilon_0\epsilon_i \times\sqrt{r^2+(z-z')^2})$$

is the bare Coulomb interaction between electrons without spin, ϵ_0 is the vacuum dielectric constant, and $\psi_i(z)$ is the wave function along the z direction in well i, $i=1$ or 2. As illustrated in Fig. 2(b), the spin introduces a nontrivial vertex $g^{\sigma,\sigma'}(\mathbf{k},\mathbf{k}+\mathbf{q})=[1+\sigma\sigma' e^{i(\phi_{\mathbf{k}}-\phi_{\mathbf{k}-\mathbf{q}})}]/2$ if the final spin polarization of electron differs from the initial one during a Coulomb collision.

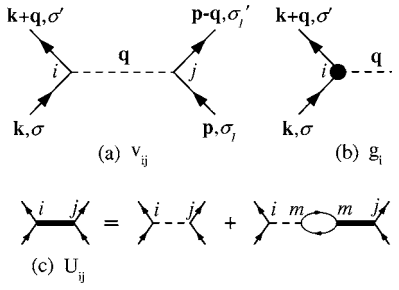

FIG. 2. Diagrammatic representation of (a) the bare Coulomb potential $v_{ij,\mathbf{k},\mathbf{p}}^{\sigma,\sigma',\sigma_1,\sigma_1'}(\mathbf{q})$, (b) the spin vertex $g_i^{\sigma,\sigma'}(\mathbf{k},\mathbf{k}+\mathbf{q})$, and (c) the RPA Dyson's equation for the screened Coulomb potential of a 2DEG $U_{ij,\mathbf{k},\mathbf{p}}^{\sigma,\sigma',\sigma_1,\sigma_1'}(\mathbf{q},\omega)$.

The technique for the multicomponent system[13,22] is used to derive the dynamically screened Coulomb potential in the random phase approximation (RPA). The following self-consistent equation is found, as illustrated diagrammatically in Fig. 2(c):

$$U_{ij,\mathbf{k},\mathbf{p}}^{\sigma,\sigma',\sigma_1,\sigma_1'}(\mathbf{q},\omega)=v_{ij,\mathbf{k},\mathbf{p}}^{\sigma,\sigma',\sigma_1,\sigma_1'}(\mathbf{q})+\sum_{\substack{\sigma_2,\sigma_2'\\ m,\mathbf{s}}}v_{im,\mathbf{k},\mathbf{s}}^{\sigma,\sigma',\sigma_2,\sigma_2'}(\mathbf{q}) \times\Pi_{m,\mathbf{s}}^{\sigma_2,\sigma_2'}(\mathbf{q},\omega)U_{mj,\mathbf{s}-\mathbf{q},\mathbf{p}}^{\sigma_2,\sigma_2',\sigma_1,\sigma_1'}(\mathbf{q},\omega). \quad (5)$$

with

$$\Pi_{i,\mathbf{k}}^{\sigma,\sigma'}(\mathbf{q},\omega)=\frac{f_i[E^{\sigma'}(\mathbf{k}+\mathbf{q})]-f_i[E^{\sigma}(\mathbf{k})]}{\hbar\omega+E^{\sigma}(\mathbf{k})-E^{\sigma'}(\mathbf{k}+\mathbf{q})+i\delta} \quad (6)$$

and f_i the Fermi distribution function in well i.

Note $U_{ij,\mathbf{k},\mathbf{p}}^{\sigma,\sigma',\sigma_1',\sigma_1'}(\mathbf{q},\omega)=g_i^{\sigma,\sigma'}(\mathbf{k},\mathbf{k}+\mathbf{q})U_{ij}(q,\omega)g_j^{\sigma_1,\sigma_1'}(\mathbf{p},\mathbf{p}-\mathbf{q})$, so the above equation reduces to

$$U_{ij}(q,\omega)=v_{ij}(q)+\sum_{\substack{\sigma_2,\sigma_2'\\ m,\mathbf{s}}}v_{im}(q)g_m^{\sigma_2,\sigma_2'}(\mathbf{s},\mathbf{s}-\mathbf{q})\Pi_{m,\mathbf{s}}^{\sigma_2,\sigma_2'}(\mathbf{q},\omega) \times g_m^{\sigma_2',\sigma_2}(\mathbf{s}-\mathbf{q},\mathbf{s})U_{mj}(q,\omega). \quad (7)$$

The elements of the corresponding 2×2 RPA dielectric matrix $\hat{\epsilon}$, defined by $v_{ij}(q)=\Sigma_m\epsilon_{im}(q,\omega)U_{mj}(q,\omega)$, reads

$$\epsilon_{ij}(q,\omega)=\delta_{ij}-v_{ij}(q)\sum_{\substack{\sigma,\sigma'\\ j,\mathbf{k}}}\frac{1}{2}\left(1+\sigma\sigma'\frac{k+q\cos\theta}{|\mathbf{k}+\mathbf{q}|}\right)\Pi_{j,\mathbf{k}}^{\sigma,\sigma'}(\mathbf{q},\omega) \quad (8)$$

with θ being the angle between $\mathbf{k}$ and $\mathbf{q}$.

III. PLASMON DISPERSION

The inverse of the dielectric matrix, $\hat{\epsilon}^{-1}$ describes the many-body response to the two-body bare Coulomb interaction v_{ij}. At the poles of $\hat{\epsilon}^{-1}$, i.e., for a set value of $(\mathbf{q},\omega)$ a particular element of $\hat{\epsilon}^{-1}$ becomes singular, a density fluctuation of the 2DEG can lead to a density oscillation in the system or the onset of a collective mode. It is well known that the zeros of the real part of the determinant of $\hat{\epsilon}$ describes the plasmon dispersion and the imaginary part the damping of the plasmon. In this paper, we discuss the plasmon spectrum by solving the equation $\mathrm{Re}|\epsilon(q,\omega)|=0$ for the 2DEG in a SQW and a DQW in the presence of RSOI.

A. Plasmons in a single well

If the coupling between 2DESs in different quantum wells is negligible, each well is independent and can be treated as a SQW. The well indices i and j drop and the dielectric matrix reduces to a scalar function

$$\epsilon(q,\omega)=1-v(q)\hat{\Pi}(\mathbf{q},\omega) \quad (9)$$

with the noninteracting correlation function

$$\hat{\Pi}(\mathbf{q},\omega)=\sum_{\sigma,\sigma'}\hat{\Pi}^{\sigma,\sigma'}(\mathbf{q},\omega)=\sum_{\sigma,\sigma',\mathbf{k}}[1+\sigma\sigma'(k+q\cos\theta)/|\mathbf{k}+\mathbf{q}|]\Pi_{\mathbf{k}}^{\sigma,\sigma'}(\mathbf{q},\omega)/2.$$

Although the RSOI splits the energy bands of different spins, the many-body Coulomb interaction between spin branches is described by a scalar dielectric function in the RPA rather than a matrix as in confinement induced multisubband systems.[22] The reason is that the RSOI does not change the wave function along the z direction and the spin vertex is separable from the no-spin Coulomb interaction as shown in Eq. (4). Equation (9) coincides with the dielectric function obtained in Refs. 8 and 11 but not with Eq. (2) in Ref. 12.

In the absence of SOI, the zero-temperature plasmon dispersion relation, frequency ω_0 vs wave vector q, is approximately expressed as

$$\omega_0^2=\frac{\hbar^2q^2\Delta^2}{4(m^*)^2(\Delta^2-1)}[4k_F^2+q^2(\Delta^2-1)] \tag{10}$$

with $\Delta=1+\pi\hbar^2/[m^*v(q)]$ and the Fermi wave vector $k_F=\sqrt{2\pi n_e}$. In the long wavelength limit $q\ll k_F$, the above equation reduces to the well-known zero-temperature 2D plasmon frequency $\omega_p=[n_e e^2q/(2\epsilon_0\epsilon_i m^*)]^{1/2}$ if the thickness of the quantum well is negligible.

In the presence of RSOI and $q\ll k_F^\sigma$, the intrabranch correlation function is given approximately by

$$\hat{\Pi}^{\sigma,\sigma}(\mathbf{q},\omega)=(1+\sigma k_\alpha/k_F^\sigma)q^2(k_F^\sigma)^2/(2\pi m^*\omega^2). \tag{11}$$

The second term is a result of the deviation of the energy band from the parabola. Since $k_F^->k_F^+$, this term leads to an extra negative term for the total intrabranch correlation $\hat{\Pi}^{++}+\hat{\Pi}^{--}$ and lowers the frequency of the plasmon. The interbranch correlation is negligible in the long wavelength limit because electron spins of the same wave vector in different branches are opposite. The long-wavelength 2D plasmon frequency with RSOI then also has a very simple dependence on the system parameters,

$$\omega_p^\alpha=\omega_p[1-k_\alpha^2/(4\pi n_e)]. \tag{12}$$

In the general case the plasmon dispersion relation is obtained numerically by searching the zeros of the real part of Eq. (9). For the sake of simplicity, only electrons in the lowest confined subband are considered and the electron wave function along the z direction is approximated by that of an infinitely high square-well potential with width $b=23$ Å, which is valid if the quantum well is not too wide. The bare Coulomb potential is then $v(q)=e^2F(qb)/(2\epsilon_0\epsilon_i q)$ with $F(\xi)=\{3\xi+8\pi^2/\xi-32\pi^4(1-e^\xi)/[\xi^2(\xi^2+\pi^2)]\}/(\xi^2+\pi^2)$.

In Fig. 3(a) we plot the plasmon spectrum and the single continuum of a 2DEG with RSOI in an InGaAs/InAlAs SQW of typical parameters appeared in recent experiments.[7] The plasmon spectrum is very close to that without SOI and it becomes difficult to distinguish one from the other. On the other hand, compared to the single continuum of the 2DEG without SOI, the single continuum with RSOI has an additional interbranch band through which the plasmon spectrum passes. The real part of the dielectric function at $q=0.2\times10^{-5}$ cm^{-1} is plotted in Fig. 3(b), whose zero near

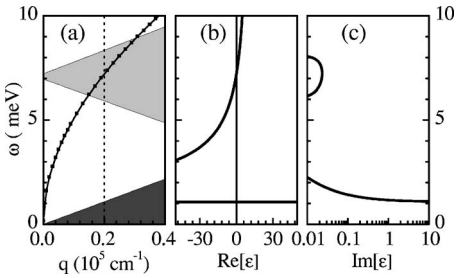

FIG. 3. (a) Plasmon spectrum of a 2DEG of density $n_e=20n_0$ in a SQW with SOI of strength $\alpha=\alpha_0$ (solid curve) and in a SQW without SOI (filled squares). Inter- (darker shaded) and intra- (light shaded) branch electron-hole continua in the presence of SOI are also shown. The vertical dashed line indicates the cross section of the spectra at $q=0.2\times10^{-5}$ cm^{-1}. (b) The real part and (c) the imaginary part of the dielectric function ϵ vs energy ω at $q=0.2\times10^{-5}$ cm^{-1}. Limited by the space, the segments of the curves for Re$[\epsilon]<-40$ in the energy range (1,3) meV, Re$[\epsilon]>40$ in (0,1), $0<$Im$[\epsilon]<0.01$ in (2.2,6.2) and (8,10], and $10<$Im$[\epsilon]$ in (0,1.1) are not shown. The temperature is $T=2$ K.

$\omega=7$ meV gives the plasmon energy and zero near $\omega=1$ meV the edge of the intrabranch single continuum. Because the spin of an electron in the upper branch is exactly opposite to that in the lower branch at the same wave vector $\mathbf{q}$, the vertical interbranch transition is not allowed under the spin-independent Coulomb interaction, and there is no zero corresponding to the edge of the interbranch single continuum. Nonvertical interbranch transitions, where the final electron wave vectors are different from the initial ones, are possible but very weak and have a negligible effect on the plasmon spectrum for $k_F\gg k_\alpha$ or high electron densities as indicated in Eq. (12) and illustrated in Fig. 3. Nevertheless, since the plasmon spectrum passes through the interbranch single continuum as shown in Fig. 3(a), the weak interbranch transitions increase the Landau damping of plasmons and lead to a nonzero imaginary part of the dielectric function in the corresponding energy range. In Fig. 3(c) the nonzero value of Im$[\epsilon]$ in the energy range (6,8.3) meV is attributed to the interbranch transitions and is much smaller than the value of Im$[\epsilon]$ inside the intrabranch single continuum in the energy range (0,1) meV.

The effect of RSOI on the 2D plasmon spectrum illustrated above coincides with that presented in Ref. 10, where the spectrum is obtained by the density-functional formalism and found to be independent of the RSOI. However, the result disagrees with the one obtained in Ref. 9, where the optical conductivity is used to evaluate the plasmon spectrum and one extra mode is observed at the edges of the interbranch single continuum. The disagreement originates from the different approaches employed. In this paper, the dynamically screened Coulomb interaction is evaluated to find the plasmon modes and the vertical transitions between the two SOI branches are not allowed under the bare Coulomb interaction. As a result, the plasmon spectrum is not greatly affected by the SOI splitting. Similarly, the independence of the plasmon spectrum of the RSOI found in Ref. 10 is a result of the fact that the charge density matrix elements vanish for vertical transitions. However, the nonvanishing

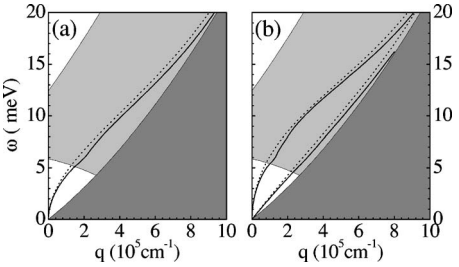

FIG. 4. Plasmon spectrum of a 2DEG without SOI (dotted curve) and with RSOI (solid curve) in a SQW (a) and in a DQW (b). The light (darker) shaded indicates the interbranch (intrabranch) electron-hole continuum in the presence of RSOI.

matrix elements of the velocity operator $\hat{\mathbf{v}}=\nabla_{\hat{\mathbf{p}}}\hat{H}$ corresponding to vertical transitions introduces a new singularity to the optical conductivity. Consequently, a new plasmon mode is predicted in Ref. 9 by an analytic treatment valid in the collision-free limit and involving order-of-magnitude estimates, see Eqs. (13) and (14) in Ref. 9. Since the validity of this formalism in the presence of RSOI is ambiguous by itself, a direct judgement on it is beyond the range of this paper. Nevertheless, experimental observations of the plasmon spectrum of electrons in a quantum well with typical parameters as used in Fig. 3 are possible to clarify the controversy.

In Fig. 4(a), we plot the plasmon dispersion relation (solid curve) as well as the single particle excitation spectrum due to intrabranch (dark shadow area) and interbranch (light gray area) transition for a 2DEG of electron density $n_e=1.5n_0$ and RSOI strength $\alpha=5\alpha_0$. For the sake of comparison, the plasmon dispersion relation in the absence of RSOI is also shown (dotted curve). We observe an overall lowering of the plasmon frequency in the presence of RSOI, which results from the RSOI modification of the band structure. Different from the case without SOI where no overlap between the plasmon and the single-excitation spectra happens in the energy range shown in Fig. 4(a), the plasmon spectrum with RSOI has a wider range of overlap with the interbranch single-excitation spectrum introduced by the RSOI spin split. Though numerical results show that the imaginary part of the dielectric function is one thousand times smaller in the interbranch single-excitation regime than that in the range of the intrabranch regime, this energy overlap can greatly enhance the Landau damping of the 2D plasmon with RSOI. Near $q=2\times10^5$ cm^{-1} where $\omega(q)\sim2\alpha k_F^+$, we notice also that a shoulder appears in the solid dispersion curve in Fig. 4(a). Its explanation is given in the following.

To have a closer look at the plasmon spectrum shift of RSOI, we define the frequency ratio ω/ω_0 as the plasmon frequency in the presence of RSOI divided by that in the absence of RSOI when other parameters are kept the same. In Fig. 5(a), the frequency ratio ω/ω_0 is plotted as a function of the RSOI strength α for various wave vectors. In the long-wavelength limit $q=0$ (solid curve), only intrabranch transitions occur and ω/ω_0 vs α follows Eq. (12). For finite q (dotted and dashed-dotted curves), interbranch transitions also affect the plasmon spectrum especially near the interbranch resonant energies at the Fermi wave vector of the $-$

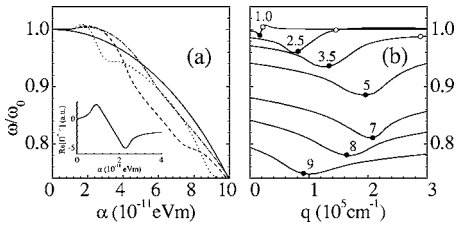

FIG. 5. (a) Frequency ratio ω/ω_0 of a SQW plasmon vs the RSOI strength α for different wave vectors $q=0$ (solid curve), 10^5 cm^{-1} (dotted curve), 2×10^5 cm^{-1} (dashed curve), and 3×10^5 cm^{-1} (dotted-dashed curve). In the inset $\hat{\Pi}^{-,+}$ vs α for $q=0.1$ and $\omega=3$ meV is shown. (b) ω/ω_0 vs q with values of α in unit of α_0 shown beside the curves. The filled (empty) circles show the resonant positions $\omega=2\alpha k_F^+$ ($2\alpha k_F^-$). The electron density is $n_e=1.5n_0$ in both panels.

branch, $\omega(q)\sim2\alpha k_F^-$, where an increase of plasmon frequency may appear, and of the $+$ branch, $\omega(q)\sim2\alpha k_F^+$, where a plasmon frequency decreases and a spectrum shoulder appears as shown in Fig. 4(a). This behavior can be understood by checking the interbranch correlation term in Eq. (8). For positive ω, $\hat{\Pi}^{+,-}(\mathbf{q},\omega)$ is negligible and $\hat{\Pi}^{-,+}(\mathbf{q},\omega)$ is approximately expressed as

$$\hat{\Pi}^{-,+}(\mathbf{q},\omega)=\sum_{\mathbf{k}}|g^{-,+}(\mathbf{k},\mathbf{k}-\mathbf{q})|^2\Pi_{\mathbf{k}}^{-,+}(\mathbf{q},\omega)$$

$$\propto q^2k_\alpha/[\tilde{k}_F(\hbar\omega-2\alpha\tilde{k}_F)], \tag{13}$$

with $k_F^+<\tilde{k}_F<k_F^-$. A numerical result of $\Pi_{\mathbf{k}}^{-,+}(\mathbf{q},\omega)$ as a function of α is shown in the inset of Fig. 5(a), which presents smoothed peaks compared to that given by Eq. (13). For strong RSOI, i.e., $2\alpha k_F^+>\omega$, $\Pi^{-,+}$ is positive and leads to an increase of plasmon frequency. If this positive interbranch correlation is larger than the RSOI negative extra term of the intrabranch correlation in Eq. (11), there will be a RSOI enhancement of the plasmon frequency. This enhancement is observed in Fig. 5(a) near $\alpha=2\alpha_0$ with $\omega/\omega_0>1$. For $2\alpha k_F^-<\omega$, $\Pi^{-,+}$ becomes negative and results in a further lowering of plasmon frequency. At fixed q, the frequency lowering of the interbranch correlation appears generally stronger than the frequency enhancement effect because it happens at larger values of α and $\Pi^{-,+}$ is proportional to α. In Fig. 5(a), the curve of $q=10^5$ cm^{-1} has two dips near $\alpha=3\alpha_0$ and $9\alpha_0$, respectively, because there are resonant energies $\omega\simeq E_{k_F^+}^+-E_{k_F^+}^-=2\alpha k_F^+$ here.

Since the plasmon frequency ω in Eq. (13) depends on the wave vector q, the frequency ratio ω/ω_0 vs q shows similar frequency enhancement and lowering as illustrated in Fig. 5(b). The effect of RSOI via intrabranch correlation is reflected in the value of ω/ω_0 at $q=0$ and the contribution via interbranch correlation is observed in the dependence on q. There is a lowering of the frequency ratio at low q and a frequency enhancement for high q. Each ω/ω_0 curve reaches its minimum (maximum) at q about $\omega(q)=2\alpha k_F^+$ ($2\alpha k_F^-$). Among the curves in Fig. 5(b), the effect of this interbranch correlation is maximum for the curve $\alpha=7\alpha_0$ whose minimum happens at the maximum value of q.

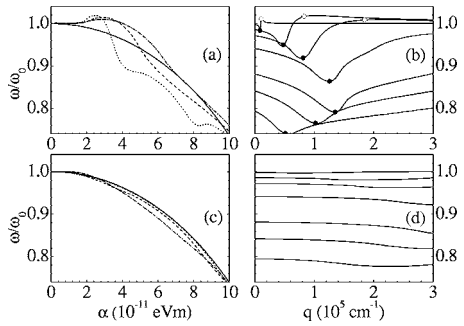

FIG. 6. Frequency ratios ω/ω_0 in a DQW as functions of α and q for the optic plasmon in (a) and (b), and the acoustic plasmon in (c) and (d). In panels (a) and (c), ω/ω_0 vs α for $q=0$ (solid), 10^5 cm^{-1} (dotted), 2×10^5 cm^{-1} (dashed), and 3×10^5 cm^{-1} (dotted-dashed) are shown. In panels (b) and (d) ω/ω_0 vs q for (from up to down) $\alpha/\alpha_0=1,2.5,3.5,5,7,8,9$ are shown. The filled (empty) circles in (b) show the resonant positions as in Fig. 5(b). The same electron density as in Fig. 5 is used.

B. Plasmons in a double well

In the DQW case, we present the results of a structure composed of two identical infinitely high quantum wells of width $b=23$ Å separated by a distance $d=175$ Å. The intrawell Coulomb interaction is $v_{11}(q)=v_{22}(q)=v(q)$ and the interwell one $v_{12}(q)=v_{21}(q)=v_d(q)=e^2e^{-qd}G(qb)/(2\epsilon_0\epsilon_i q)$ with $G(\xi)=16\pi^4(1-e^{\xi})e^{-\xi}/[\xi^2(\xi^2+\pi^2)^2]$. The plasmon spectrum is given by the zeros of the determinant of the dielectric matrix. From Eq. (8), the determinant is expressed as

$$|\hat{\epsilon}| = (1-v\hat{\Pi}_1)(1-v\hat{\Pi}_2) - v_d^2\hat{\Pi}_1\hat{\Pi}_2 \tag{14}$$

with $\hat{\Pi}_i$ the noninteracting correlation function in well i. In general, two plasmon modes, the optic mode of higher energy and the acoustic mode, are obtained out of the single particle excitation spectrum. If the electron densities in both wells are the same, Eq. (10) is still valid in the absence of RSOI for the zero-temperature plasmon dispersion by replacing Δ with $\Delta_{\rm op}=v+v_d$ for the optic mode and $\Delta_{\rm ac}=v-v_d$ for the acoustic mode. In the long-wavelength limit, the frequency of the optic mode is about $\omega_p^{\rm op}=\sqrt{2}\omega_p$ and that of the acoustic mode $\omega_p^{\rm ac}=(n_e e^2 d/2\epsilon_0\epsilon_i m^*)^{1/2}q$.

In the numerical calculation, the plasmon dispersion is obtained by obtaining the zeros of the real part of the determinant of the dielectric matrix $\mathrm{Re}|\hat{\epsilon}(q,\omega)|$. A typical plasmon dispersion of 2DEG in a DQW with RSOI is illustrated in Fig. 4(b). As in the SQW, the dispersion curve of each plasmon mode is generally lowered by RSOI via intrabranch correlations and has a shoulder at the resonant energy $2\alpha k_F^+$ of interbranch transitions for electrons near the inner Fermi circle. Compared with the shoulder of the SQW plasmon spectrum in Fig. 4(a), the shoulder for the optic mode happens at a lower wave vector by a factor $1/\sqrt{2}$ and has an enhanced amplitude but that for the acoustic mode is almost dispensable. We plot the RSOI strength dependence of the frequency ratio for the optic mode in Fig. 6(a) and for the acoustic mode in Fig. 6(c). Both modes have the same dependence on α in the long wavelength limit $q=0$ as expressed by Eq. (12). At finite wave vector, the frequency ratio shows strong deviation from that of $q=0$ for the optic mode but it is not the case for the acoustic mode. To see more clearly the dependence of ω/ω_0 on q, the DQW frequency ratio ω/ω_0 vs wave vector q for optic and acoustic modes are plotted in Figs. 6(b) and 6(d), respectively with RSOI strength $\alpha=1,2.5,3.5,5,7,8,9\alpha_0$ for curves counted from top. The curves of the optic mode are similar to those of the SQW plasmon with minima near $\omega(q)=2\alpha k_F^+$ and maxima near $2\alpha k_F^-$. Because the DQW optic mode has a higher energy than the SQW mode, the minima shift to lower q values by a factor of $1/\sqrt{2}$. The frequency ratio of the DQW acoustic plasmon mode, however, has a very weak dependence on wave vector. Interbranch transitions can lower the optic plasmon frequency more than 10% and the acoustic plasmon frequency less than 3%.

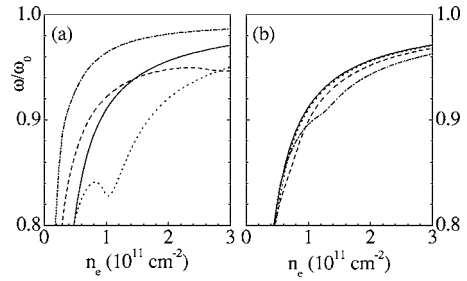

FIG. 7. ω/ω_0 of (a) the optic and (b) the acoustic plasmons vs n_e in a DQW with $\alpha/\alpha_0=5$. Results of $q=0$ (solid), 10^5 cm^{-1} (dotted), 2×10^5 cm^{-1} (dashed), and 3×10^5 cm^{-1} (dotted-dashed) are shown.

The electron density dependence of the frequency ratio ω/ω_0 is plotted for the optic mode in Fig. 7(a) and the acoustic mode in Fig. 7(b) in a wave vector range up to $q=3\times10^5$ cm^{-1}. In the long-wavelength limit $q=0$, it is described by Eq. (11) for both modes. Fine structure appears in finite q as interbranch transitions are switched on. For the optic mode, with increasing wave vector, the ratio decreases at first and a dip appear about $\omega=2\alpha k_F^+$ which is $n_e=n_0$ for $q=10^5$ cm^{-1}. Then the ratio increases from the low-density regime to the higher-density regime. At $q=3$ it is higher than the value of $q=0$ over the whole regime. For the acoustic mode, on the other hand, the ratio ω/ω_0 decreases and then increases with q in the low-density regime but keeps decreasing up to $q=3$ in the higher density regime. The overall ratio at finite wave vectors is lower than that in the zero-wave-vector limit. For $n_e>3n_0$, all the curves ω/ω_0 in Fig. 7 are above 0.94 and converge to 1 with increasing n_e.

Note that our results are obtained in the RPA which may break down in systems of low electron density or systems at high temperature. The validity of the RPA can be justified by the parameter r_s defined by $n_e^{-1}=\pi r_s^2 a_B^{*2}$ with the effective Bohr radius $a_B^*=4\pi\epsilon_0\epsilon_\infty\hbar^2/(m^*e^2)$. For a 2DES of electron density n_0, which corresponds to $r_s\approx1.6$ here, the RPA is still valid at low temperature. Experiments also indicate that the RPA describes the plasmon spectrum and the Coulomb drag of 2DEGs reasonably well at low temperature in GaAs/AlGaAs systems with electron density of order n_0.[16,19,21] For a system of lower electron density or at higher temperature, the local-field correction to the dielectric function and the plasmon spectrum of 2DEGs becomes more important.[19,20,23,24]

IV. CONCLUDING REMARKS

In the framework of the random phase approximation, we studied the dielectric function and the plasmon spectrum of single and coupled 2DEGs with RSOI in GaInAs-based semiconductor structures. In the SQW case, the RSOI lifts the spin degeneracy of electrons of finite wave vector but does not change the spatial wave functions when the spin orientation of a electron varies. Thus the bare Coulomb coupling between the electrons is not affected by the RSOI though the spin effect to this coupling should be considered explicitly in the presence of RSOI. The screened Coulomb coupling and the dielectric function, nevertheless, are modified by RSOI because the electron correlation in the system varies with the energy-band shape. As a result of the invariance of spatial wave function of electrons in different spin branches, the dielectric function describing the Coulomb coupling between electrons in different spin branches has the same form and the system is a single-component system. The deformation of the energy band from a parabola for each spin branch results in a negative term of intrabranch contributions to the dielectric function, which lowers the plasmon frequency. The frequency decrease is proportional to the square of the RSOI strength and the inverse of the electron density in the long wavelength limit. At finite wave vector of the plasmon, the contribution of interbranch transitions to the dielectric function is negative at energy lower than the spin split of the inner Fermi circle and positive at energy higher than the spin split of the outer Fermi circle. This leads to a shoulder in the plasmon dispersion curve at the energy equal to the spin split of the inner Fermi circle and a possible RSOI frequency enhancement for plasmon of higher energy dependent on the competition between the intra- and interbranch contributions.

In DQW systems, a similar influence of RSOI via intrabranch transitions is observed on both the optic and acoustic modes. The effect of RSOI via interbranch transitions is enhanced (diminished) for the optic (acoustic) mode. The interbranch single-particle excitation spectrum covers part of the plasmon spectrum and leads to the Landau damping of plasmons.

ACKNOWLEDGMENTS

The author thanks P. Vasilopoulos, W. Xu, and M. S. Kushwaha for helpful discussions. This work was supported by the Canadian NSERC Grant No. OGP0121756.

*Electronic address: xuefeng@alcor.concordia.ca

[1] S. Datta and B. Das, Appl. Phys. Lett. **56**, 665 (1990).
[2] X. F. Wang, P. Vasilopoulos, and F. M. Peeters, Phys. Rev. B **65**, 165217 (2002).
[3] G. Dresselhaus, Phys. Rev. **100**, 580 (1955).
[4] Y. A. Bychkov and E. I. Rashba, JETP Lett. **39**, 78 (1984).
[5] L. Vervoort, R. Ferreira, and P. Voisin, Phys. Rev. B **56**, R12744 (1997).
[6] U. Rossler and J. Kainz, Solid State Commun. **121**, 313 (2002).
[7] See, for example, J. Luo, H. Munekata, F. F. Fang, and P. J. Stiles, Phys. Rev. B **38**, 10142 (1988); T. Koga, J. Nitta, T. Akazaki, and H. Takayanagi, Phys. Rev. Lett. **89**, 046801 (2002).
[8] G. H. Chen and M. E. Raikh, Phys. Rev. B **59**, 5090 (1999).
[9] L. I. Magarill, A. V. Chaplik, and M. V. Éntin, JETP **92**, 153 (2001).
[10] C. A. Ullrich and M. E. Flatté, Phys. Rev. B **66**, 205305 (2002).
[11] E. G. Mishchenko and B. I. Halperin, Phys. Rev. B **68**, 045317 (2003).
[12] W. Xu, Appl. Phys. Lett. **82**, 724 (2003).
[13] S. Das Sarma and A. Madhukar, Phys. Rev. B **23**, 805 (1981).
[14] G. E. Santoro and G. F. Giuliani, Phys. Rev. B **37**, 937 (1988).
[15] G. Fasol, N. Mestres, H. P. Hughes, A. Fischer, and K. Ploog, Phys. Rev. Lett. **56**, 2517 (1986).
[16] D. S. Kainth, D. Richards, A. S. Bhatti, H. P. Hughes, M. Y. Simmons, E. H. Linfield, and D. A. Ritchie, Phys. Rev. B **59**, 2095 (1999).
[17] C.-M. Hu, C. Schüller, and D. Heitmann, Phys. Rev. B **64**, 073303 (2001).
[18] K. Flensberg and BenYu-Kuang Hu, Phys. Rev. Lett. **73**, 3572 (1994).
[19] N. P. R. Hill, J. T. Nicholls, E. H. Linfield, M. Pepper, D. A. Ritchie, G. A. C. Jones, BenYu-Kuang Hu, and K. Flensberg, Phys. Rev. Lett. **78**, 2204 (1997).
[20] A. G. Rojo, J. Phys.: Condens. Matter **11**, R31 (1999).
[21] X. F. Wang and I. C. da Cunha Lima, Phys. Rev. B **63**, 205312 (2001).
[22] B. Vinter, Phys. Rev. B **15**, 3947 (1977).
[23] L. Zheng and A. H. MacDonald, Phys. Rev. B **49**, 5522 (1994).
[24] S. Das Sarma and E. H. Hwang, Phys. Rev. Lett. **81**, 4216 (1998).